

The IceCube Neutrino Observatory V: Future Developments

THE ICECUBE COLLABORATION

1. Status and recent results of the South Pole Acoustic Test Setup	1
2. The Radio Air Shower Test Array (RASTA) – enhancing the IceCube observatory	5
3. IceCube’s In Ice Radio-Frequency extension	9
4. First Step towards A New Proton Decay Experiment In Ice	13

Keywords: *IceCube, SPATS, ARA, RASTA, acoustic neutrino detection, acoustic ice properties, radio air shower detection, neutrino, Askaryan, ice properties, GZK, attenuation, proton decay, GENIE, GPGPU photon tracking*



IceCube Collaboration Member List

R. ABBASI²⁸, Y. ABDOU²², T. ABU-ZAYYAD³³, M. ACKERMANN³⁹, J. ADAMS¹⁶, J. A. AGUILAR²⁸, M. AHLERS³², M. M. ALLEN³⁶, D. ALTMANN¹, K. ANDEEN^{28,a}, J. AUFFENBERG³⁸, X. BAI^{31,b}, M. BAKER²⁸, S. W. BARWICK²⁴, R. BAY⁷, J. L. BAZO ALBA³⁹, K. BEATTIE⁸, J. J. BEATTY^{18,19}, S. BECHET¹³, J. K. BECKER¹⁰, K.-H. BECKER³⁸, M. L. BENABDERRAHMANE³⁹, S. BENZVI²⁸, J. BERDERMANN³⁹, P. BERGHAUS³¹, D. BERLEY¹⁷, E. BERNARDINI³⁹, D. BERTRAND¹³, D. Z. BESSON²⁶, D. BINDIG³⁸, M. BISSOK¹, E. BLAUFUSS¹⁷, J. BLUMENTHAL¹, D. J. BOERSMA¹, C. BOHM³⁴, D. BOSE¹⁴, S. BÖSER¹¹, O. BOTNER³⁷, A. M. BROWN¹⁶, S. BUITINK¹⁴, K. S. CABALLERO-MORA³⁶, M. CARSON²², D. CHIRKIN²⁸, B. CHRISTY¹⁷, F. CLEVERMANN²⁰, S. COHEN²⁵, C. COLNARD²³, D. F. COWEN^{36,35}, A. H. CRUZ SILVA³⁹, M. V. D'AGOSTINO⁷, M. DANNINGER³⁴, J. DAUGHHETEE⁵, J. C. DAVIS¹⁸, C. DE CLERCQ¹⁴, T. DEGNER¹¹, L. DEMIRÖRS²⁵, F. DESCAMPS²², P. DESIATI²⁸, G. DE VRIES-UITERWEERD²², T. DEYOUNG³⁶, J. C. DÍAZ-VÉLEZ²⁸, M. DIERCKXSENS¹³, J. DREYER¹⁰, J. P. DUMM²⁸, M. DUNKMAN³⁶, J. EISCH²⁸, R. W. ELLSWORTH¹⁷, O. ENGDEGÅRD³⁷, S. EULER¹, P. A. EVENSON³¹, O. FADIRAN²⁸, A. R. FAZELY⁶, A. FEDYNITCH¹⁰, J. FEINTZEIG²⁸, T. FEUSELS²², K. FILIMONOV⁷, C. FINLEY³⁴, T. FISCHER-WASELS³⁸, B. D. FOX³⁶, A. FRANCKOWIAK¹¹, R. FRANKE³⁹, T. K. GAISSER³¹, J. GALLAGHER²⁷, L. GERHARDT^{8,7}, L. GLADSTONE²⁸, T. GLÜSENKAMP³⁹, A. GOLDSCHMIDT⁸, J. A. GOODMAN¹⁷, D. GÓRA³⁹, D. GRANT²¹, T. GRIESEL²⁹, A. GROSS^{16,23}, S. GRULLON²⁸, M. GURTNER³⁸, C. HA³⁶, A. HAJ ISMAIL²², A. HALLGREN³⁷, F. HALZEN²⁸, K. HAN³⁹, K. HANSON^{13,28}, D. HEINEN¹, K. HELBING³⁸, R. HELLAUER¹⁷, S. HICKFORD¹⁶, G. C. HILL²⁸, K. D. HOFFMAN¹⁷, A. HOMEIER¹¹, K. HOSHINA²⁸, W. HUELSNIETZ^{17,c}, J.-P. HÜLSS¹, P. O. HULTH³⁴, K. HULTQVIST³⁴, S. HUSSAIN³¹, A. ISHIHARA¹⁵, E. JACOBI³⁹, J. JACOBSEN²⁸, G. S. JAPARIDZE⁴, H. JOHANSSON³⁴, K.-H. KAMPERT³⁸, A. KAPPES⁹, T. KARG³⁸, A. KARLE²⁸, P. KENNY²⁶, J. KIRYLUK^{8,7}, F. KISLAT³⁹, S. R. KLEIN^{8,7}, J.-H. KÖHNE²⁰, G. KOHNEN³⁰, H. KOLANOSKI⁹, L. KÖPKE²⁹, S. KOPPER³⁸, D. J. KOSKINEN³⁶, M. KOWALSKI¹¹, T. KOWARIK²⁹, M. KRASBERG²⁸, T. KRINGS¹, G. KROLL²⁹, N. KURAHASHI²⁸, T. KUWABARA³¹, M. LABARE¹⁴, K. LAIHEM¹, H. LANDSMAN²⁸, M. J. LARSON³⁶, R. LAUER³⁹, J. LÜNEMANN²⁹, J. MADSEN³³, A. MAROTTA¹³, R. MARUYAMA²⁸, K. MASE¹⁵, H. S. MATIS⁸, K. MEAGHER¹⁷, M. MERCK²⁸, P. MÉSZÁROS^{35,36}, T. MEURES¹³, S. MIARECKI^{8,7}, E. MIDDELL³⁹, N. MILKE²⁰, J. MILLER³⁷, T. MONTARULI^{28,d}, R. MORSE²⁸, S. M. MOVIT³⁵, R. NAHNHAUER³⁹, J. W. NAM²⁴, U. NAUMANN³⁸, D. R. NYGREN⁸, S. ODROWSKI²³, A. OLIVAS¹⁷, M. OLIVO¹⁰, A. O'MURCHADHA²⁸, S. PANKNIN¹¹, L. PAUL¹, C. PÉREZ DE LOS HEROS³⁷, J. PETROVIC¹³, A. PIEGSA²⁹, D. PIELOTH²⁰, R. PORRATA⁷, J. POSSELT³⁸, P. B. PRICE⁷, G. T. PRZYBYLSKI⁸, K. RAWLINS³, P. REDL¹⁷, E. RESCONI^{23,e}, W. RHODE²⁰, M. RIBORDY²⁵, M. RICHMAN¹⁷, J. P. RODRIGUES²⁸, F. ROTHMAIER²⁹, C. ROTT¹⁸, T. RUHE²⁰, D. RUTLEDGE³⁶, B. RUZYBAYEV³¹, D. RYCKBOSCH²², H.-G. SANDER²⁹, M. SANTANDER²⁸, S. SARKAR³², K. SCHATTO²⁹, T. SCHMIDT¹⁷, A. SCHÖNWALD³⁹, A. SCHUKRAFT¹, A. SCHULTES³⁸, O. SCHULZ^{23,f}, M. SCHUNCK¹, D. SECKEL³¹, B. SEMBURG³⁸, S. H. SEO³⁴, Y. SESTAYO²³, S. SEUNARINE¹², A. SILVESTRI²⁴, G. M. SPICZAK³³, C. SPIERING³⁹, M. STAMATIKOS^{18,g}, T. STANEV³¹, T. STEZELBERGER⁸, R. G. STOKSTAD⁸, A. STÖSSL³⁹, E. A. STRAHLER¹⁴, R. STRÖM³⁷, M. STÜER¹¹, G. W. SULLIVAN¹⁷, Q. SWILLENS¹³, H. TAAVOLA³⁷, I. TABOADA⁵, A. TAMBURRO³³, A. TEPE⁵, S. TER-ANTONYAN⁶, S. TILAV³¹, P. A. TOALE², S. TOSCANO²⁸, D. TOSI³⁹, N. VAN EIJDHOVEN¹⁴, J. VANDENBROUCKE⁷, A. VAN OVERLOOP²², J. VAN SANTEN²⁸, M. VEHRING¹, M. VOGEL¹¹, C. WALCK³⁴, T. WALDENMAIER⁹, M. WALLRAFF¹, M. WALTER³⁹, CH. WEAVER²⁸, C. WENDT²⁸, S. WESTERHOFF²⁸, N. WHITEHORN²⁸, K. WIEBE²⁹, C. H. WIEBUSCH¹, D. R. WILLIAMS², R. WISCHNEWSKI³⁹, H. WISSING¹⁷, M. WOLF²³, T. R. WOOD²¹, K. WOSCHNAGG⁷, C. XU³¹, D. L. XU², X. W. XU⁶, J. P. YANEZ³⁹, G. YODH²⁴, S. YOSHIDA¹⁵, P. ZARZHITSKY², M. ZOLL³⁴

-
- ¹*III. Physikalisches Institut, RWTH Aachen University, D-52056 Aachen, Germany*
²*Dept. of Physics and Astronomy, University of Alabama, Tuscaloosa, AL 35487, USA*
³*Dept. of Physics and Astronomy, University of Alaska Anchorage, 3211 Providence Dr., Anchorage, AK 99508, USA*
⁴*CTSPS, Clark-Atlanta University, Atlanta, GA 30314, USA*
⁵*School of Physics and Center for Relativistic Astrophysics, Georgia Institute of Technology, Atlanta, GA 30332, USA*
⁶*Dept. of Physics, Southern University, Baton Rouge, LA 70813, USA*
⁷*Dept. of Physics, University of California, Berkeley, CA 94720, USA*
⁸*Lawrence Berkeley National Laboratory, Berkeley, CA 94720, USA*
⁹*Institut für Physik, Humboldt-Universität zu Berlin, D-12489 Berlin, Germany*
¹⁰*Fakultät für Physik & Astronomie, Ruhr-Universität Bochum, D-44780 Bochum, Germany*
¹¹*Physikalisches Institut, Universität Bonn, Nussallee 12, D-53115 Bonn, Germany*
¹²*Dept. of Physics, University of the West Indies, Cave Hill Campus, Bridgetown BB11000, Barbados*
¹³*Université Libre de Bruxelles, Science Faculty CP230, B-1050 Brussels, Belgium*
¹⁴*Vrije Universiteit Brussel, Dienst ELEM, B-1050 Brussels, Belgium*
¹⁵*Dept. of Physics, Chiba University, Chiba 263-8522, Japan*
¹⁶*Dept. of Physics and Astronomy, University of Canterbury, Private Bag 4800, Christchurch, New Zealand*
¹⁷*Dept. of Physics, University of Maryland, College Park, MD 20742, USA*
¹⁸*Dept. of Physics and Center for Cosmology and Astro-Particle Physics, Ohio State University, Columbus, OH 43210, USA*
¹⁹*Dept. of Astronomy, Ohio State University, Columbus, OH 43210, USA*
²⁰*Dept. of Physics, TU Dortmund University, D-44221 Dortmund, Germany*
²¹*Dept. of Physics, University of Alberta, Edmonton, Alberta, Canada T6G 2G7*
²²*Dept. of Physics and Astronomy, University of Gent, B-9000 Gent, Belgium*
²³*Max-Planck-Institut für Kernphysik, D-69177 Heidelberg, Germany*
²⁴*Dept. of Physics and Astronomy, University of California, Irvine, CA 92697, USA*
²⁵*Laboratory for High Energy Physics, École Polytechnique Fédérale, CH-1015 Lausanne, Switzerland*
²⁶*Dept. of Physics and Astronomy, University of Kansas, Lawrence, KS 66045, USA*
²⁷*Dept. of Astronomy, University of Wisconsin, Madison, WI 53706, USA*
²⁸*Dept. of Physics, University of Wisconsin, Madison, WI 53706, USA*
²⁹*Institute of Physics, University of Mainz, Staudinger Weg 7, D-55099 Mainz, Germany*
³⁰*Université de Mons, 7000 Mons, Belgium*
³¹*Bartol Research Institute and Department of Physics and Astronomy, University of Delaware, Newark, DE 19716, USA*
³²*Dept. of Physics, University of Oxford, 1 Keble Road, Oxford OX1 3NP, UK*
³³*Dept. of Physics, University of Wisconsin, River Falls, WI 54022, USA*
³⁴*Oskar Klein Centre and Dept. of Physics, Stockholm University, SE-10691 Stockholm, Sweden*
³⁵*Dept. of Astronomy and Astrophysics, Pennsylvania State University, University Park, PA 16802, USA*
³⁶*Dept. of Physics, Pennsylvania State University, University Park, PA 16802, USA*
³⁷*Dept. of Physics and Astronomy, Uppsala University, Box 516, S-75120 Uppsala, Sweden*
³⁸*Dept. of Physics, University of Wuppertal, D-42119 Wuppertal, Germany*
³⁹*DESY, D-15735 Zeuthen, Germany*
^a*now at Dept. of Physics and Astronomy, Rutgers University, Piscataway, NJ 08854, USA*
^b*now at Physics Department, South Dakota School of Mines and Technology, Rapid City, SD 57701, USA*
^c*Los Alamos National Laboratory, Los Alamos, NM 87545, USA*
^d*also Sezione INFN, Dipartimento di Fisica, I-70126, Bari, Italy*
^e*now at T.U. Munich, 85748 Garching & Friedrich-Alexander Universität Erlangen-Nürnberg, 91058 Erlangen, Germany*
^f*now at T.U. Munich, 85748 Garching, Germany*
^g*NASA Goddard Space Flight Center, Greenbelt, MD 20771, USA*

Acknowledgments

We acknowledge the support from the following agencies: U.S. National Science Foundation–Office of Polar Programs, U.S. National Science Foundation–Physics Division, University of Wisconsin Alumni Research Foundation, the Grid Laboratory Of Wisconsin (GLOW) grid infrastructure at the University of Wisconsin - Madison, the Open Science Grid (OSG) grid infrastructure; U.S. Department of Energy, and National Energy Research Scientific Computing Center, the Louisiana Optical Network Initiative (LONI) grid computing resources; National Science and Engineering Research Council of Canada; Swedish Research Council, Swedish Polar Research Secretariat, Swedish National Infrastructure for Computing

(SNIC), and Knut and Alice Wallenberg Foundation, Sweden; German Ministry for Education and Research (BMBF), Deutsche Forschungsgemeinschaft (DFG), Research Department of Plasmas with Complex Interactions (Bochum), Germany; Fund for Scientific Research (FNRS-FWO), FWO Odysseus programme, Flanders Institute to encourage scientific and technological research in industry (IWT), Belgian Federal Science Policy Office (Belspo); University of Oxford, United Kingdom; Marsden Fund, New Zealand; Japan Society for Promotion of Science (JSPS); the Swiss National Science Foundation (SNSF), Switzerland; D. Boersma acknowledges support by the EU Marie Curie IRG Program; A. Groß acknowledges support by the EU Marie Curie OIF Program; J. P. Rodrigues acknowledges support by the Capes Foundation, Ministry of Education of Brazil; A. Schukraft acknowledges the support by the German Telekom Foundation; N. Whitehorn acknowledges support by the NSF Graduate Research Fellowships Program.



Status and recent results of the South Pole Acoustic Test Setup

THE ICECUBE COLLABORATION¹

¹See special section in these proceedings

Abstract: The feasibility and design of an acoustic neutrino detection array in the South Pole ice depend on the acoustic properties of the ice. The South Pole Acoustic Test Setup (SPATS) was built to evaluate the acoustic characteristics of the ice in the 10 to 100 kHz frequency range. SPATS has been operating successfully since January 2007 and has been able to measure or constrain all parameters. Recent results including the absolute noise measurement of the South Pole ice, the SPATS sensor calibration, and the frequency dependence of attenuation length are presented.

Corresponding authors: Yasser Abdou (yasser@inwfsun1.ugent.be)
Department of Physics and Astronomy, Gent University, B-9000 Gent, Belgium

Keywords: Acoustic neutrino detection, Acoustic ice properties, SPATS

1 Introduction

The detection of ultra-high energy neutrinos of extraterrestrial origin is a big challenge because of their low flux and small interaction cross-sections. To detect the cosmogenic or Greisen-Zatsepin-Kuzmin (GZK), neutrinos of energy 10^{17-20} eV produced by ultra-high-energy cosmic rays interacting with the cosmic microwave background radiation, a detector with effective volume in the order of 100 km^3 is needed. Such a large volume is necessary since the estimated rate of GZK neutrino induced showers is on the order of $0.1 \text{ km}^{-3}\text{yr}^{-1}$ [1, 2].

The interactions of high energy neutrinos in ice produce optical [3], radio [4], and acoustic radiation [5], each of which therefore provides a possible method of detecting the neutrinos. Both radio and acoustic signals have attenuation lengths that are larger than in the optical signals [6].

While the optical method is well understood and calibrated with atmospheric neutrinos, the density of instrumentation required makes it prohibitively expensive to scale to a 100 km^3 detector size. The acoustic and radio methods, on the other hand, can in principle be used to instrument a large volume sparsely and achieve good sensitivity per cost in this energy range [8].

South Pole ice as a medium is predicted to be especially well suited for acoustic detection of extremely high-energy neutrinos [7]. To test the theoretical estimates, the South Pole Acoustic Test Setup (SPATS) was deployed at the South Pole. The main purpose of SPATS is to measure the acoustic attenuation length, sound speed profile, noise

floor, and transient noise sources in situ at the South Pole. Measurement of these parameters will allow us to obtain a realistic sensitivity estimate for a possible future acoustic neutrino telescope in the Antarctic ice.

2 SPATS Array

The South Pole Acoustic Test Setup consists of four vertical strings that were deployed in the upper 500 meters of selected IceCube holes to form a trapezoidal array, with inter-string distances from 125 to 543 m [9]. Each string has 7 acoustic stages, each stage is comprised of a sensor and a transmitter. The transmitter module consists of a steel pressure vessel that houses a high-voltage pulse generator board and a temperature or pressure sensor. Triggered HV pulses are sent to the transmitter, a ring-shaped piezo-ceramic element that is cast in epoxy for electrical insulation and positioned 13 cm below the steel housing. The motivation of using ring-shaped piezo-ceramics is to obtain an azimuthally isotropic emission. The actual emission directivity of such an element was measured in the azimuthal and polar directions [10]. The sensor module has three channels, each 120° apart in azimuth, to ensure good angular coverage.

A retrievable pinger was also deployed in 13 water-filled IceCube holes: 6 holes were pinged in December 2007-January 2008 and 7 more holes were pinged using an improved pinger design; 4 in December 2008-January 2009 and 3 in December 2009-January 2010. In 2009/2010, the pinger was modified to emit lower bandwidth pulses at

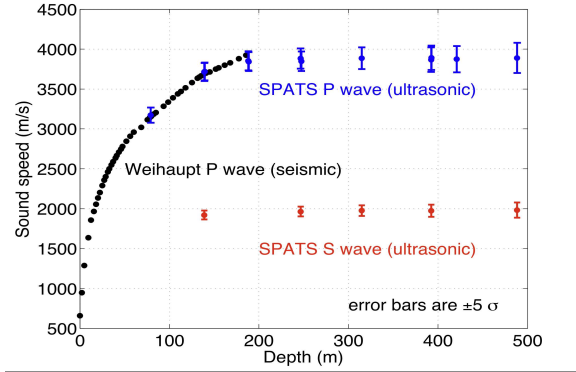


Figure 1: Sound speed for both pressure and shear waves, at ultrasonic frequencies, versus depth in the South Pole ice. A previous measurement, made by Weihaupt, at seismic (Hz) frequencies is shown for comparison [11].

three well defined frequencies (30, 45, and 60 kHz) and deployed in three boreholes going down to 1000 m depth. The measured data is used to study the frequency dependence of the attenuation length, as well as the speed of sound on inclined paths.

3 Results

3.1 Sound speed

The speed of both pressure waves and shear waves are measured in the dense ice between 80 m and 500 m as a function of depth using the SPATS pinger setup [11], and were found to be 3878 ± 12 m/s and 1975.8 ± 8.0 m/s, respectively. The resulting vertical sound speed gradient for both pressure and shear waves is consistent with no refraction between 200 and 500 m depth as shown in Fig. 1. These results have encouraging implications for neutrino astronomy: the negligible refraction of acoustic waves deeper than 200 m indicates that neutrino direction and energy reconstruction, as well as separation from background events, could be done easily and accurately.

3.2 Properties of noise floor

The energy threshold for the detection of acoustic signals from ultra-high energy neutrino interactions depends strongly on the absolute noise level in the target material. SPATS has monitored the noise in Antarctic ice at the geographic South Pole for more than two years down to 500 m depth. The noise is very stable and Gaussian distributed as shown in Fig. 2 [12]. The resulting noise level for all operative SPATS channels is presented in ref. [12]. The contribution from electronic self-noise that has been measured in the laboratory prior to deployment is found to be 7 mPa. Subtracting this contribution quadratically from the measured mean noise level leads to an estimated mean noise level in South Polar ice of 20 mPa above 200 m and 14 mPa

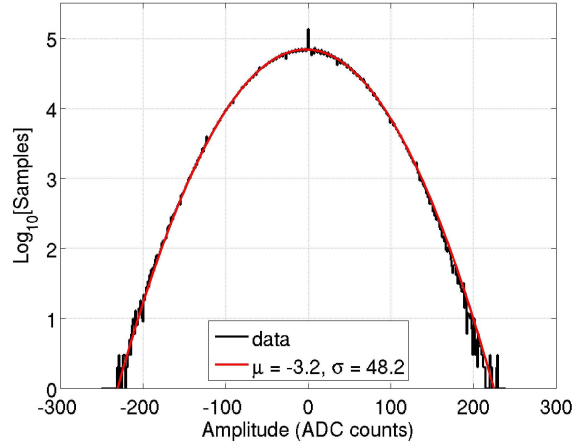


Figure 2: An example for the South Pole noise floor recorded by one of the SPATS sensors.

below 200 m integrated over the frequency range relevant for acoustic neutrino detection of 10 to 50 kHz. The origin and significance of the decrease in the noise level with depth remains unclear. One possible qualitative explanation for the observed depth dependence is a contribution of noise generated on the surface. Due to the gradient in the sound speed with depth [11], all noise from the surface will be refracted back towards the surface, thus shielding deeper regions from surface noise.

3.3 Transient noise events

Using a threshold trigger mode for the active SPATS channels and offline coincidence window of 200 ms, corresponding to a pressure wave with the longest distance across the SPATS array of approximately 775 m, the vertex of transient events producing triggers on all four strings is reconstructed using an idealized global positioning system algorithm [12]. The horizontal positions of all reconstructed vertices are shown in Fig. 3. SPATS registered acoustic pulse-like events in the IceCube detector volume and its vicinity. All sources of transient noise are well localized in space and have been identified as being man made; IceCube boreholes re-freezing after the deployment of the optical module produce cracking noise for a period of about 20 days. Rodriguez Wells, caverns melted in the ice at a depth of 50-100 m as a water source for IceCube drilling, also produce a cracking noise during refreezing.

The acoustic signals from refreezing IceCube holes and from anthropogenic sources have been used to localize acoustic events. The absence of any transient events observed from locations other than known sources allows us to set a limit on the flux of ultra high energy ($E_\nu > 10^{20}$ eV) neutrinos. Fig. 4 shows the neutrino flux limit of the 2009 SPATS configuration (70 mPa threshold, ≥ 5 hits per event) compared to different neutrino flux limits [12].

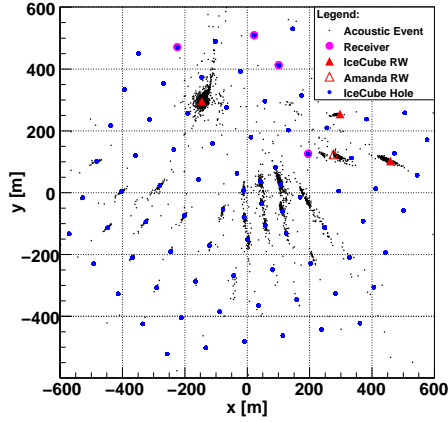


Figure 3: The vertex position for all transient events recorded since August 2008 in the horizontal plane of the the IceCube coordinate system, see the original figure from Ref. [12].

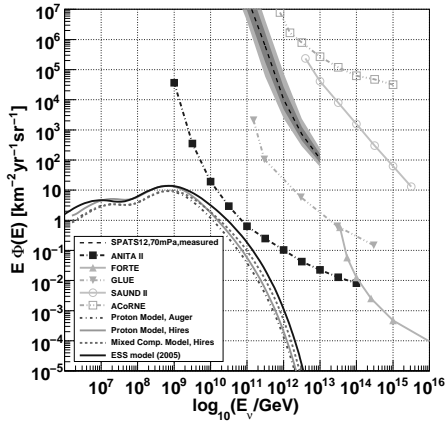


Figure 4: The neutrino flux limit of the 2009 SPATS configuration (70 mPa threshold, ≥ 5 hits per event), for the detailed description of the limits see Ref. [12].

3.4 Attenuation length

Measuring the attenuation length requires the comparison of signal amplitudes or energies after different propagation lengths through the ice. To achieve this, the 2008/2009 pinger was equipped with mechanical stabilizers, in order to keep the pinger close to the central axis of the hole. Centralization of the pinger minimized pulse to pulse variations caused by different signal transmission characteristics at the water-ice interface. The pinger emission rate was increased from 1 Hz (used in the previous season) to 10 Hz in order to improve the signal to noise ratio.

The data sets from 2008/2009 were analyzed using different sound sources, the pinger, the frozen-in SPATS transmitters and transient signals from freezing IceCube holes to determine the attenuation length. To minimize the uncertainties due to different sensitivity of the sensors and

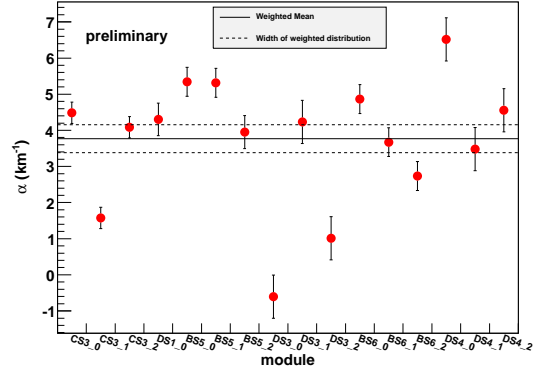


Figure 5: The attenuation coefficients with standard error for different SPATS sensors at 30 kHz.

unknown angular response, the attenuation length was determined with each sensor individually placing the sound source at different distances to the receiver, while trying to keep the same direction seen from the sensor. All methods consistently deliver an attenuation length of about 300 m with a 20% uncertainty [13]. These measurements observed a weak frequency dependence below 30 kHz. This result is in strong contradiction with the phenomenological model prediction of 9 ± 3 km with absorption as the dominant mechanism and negligible scattering on ice grains [7].

To investigate this discrepancy the pinger was modified for the 2009/2010 Pole season to allow us to measure the attenuation length at different frequencies from 30 kHz to 60 kHz. The result will help to discriminate between different contributing attenuation mechanisms: the scattering coefficient is expected to increase with f^4 while the absorption coefficient should be nearly frequency independent. The modified pinger was successfully deployed in three IceCube holes aligned with respect to the SPATS array at horizontal distances between 180 m and 820 m and delivered high quality data.

Each waveform consists of six pulses, two sets of 3 pulses in a (30,45,60) kHz cycle. The energy contribution from the noise-subtracted waveform was calculated at each frequency in order to calculate the attenuation coefficient as explained in [13]. Fig. 5 shows the attenuation coefficient as obtained from the available horizontal pinger-sensor configuration at a frequency of 30 kHz. The data points scatter more than their error bars indicate, implying that there are additional systematic uncertainties, e.g. arising from local ice properties or the interface between the hole ice and the sensors. The error represents the spread between attenuation lengths measured with each sensor. The weighted mean for the attenuation length is 266 ± 27 m at 30 kHz and 300 ± 88 m at 45 kHz. The contribution of 60 kHz is not strong enough at large distances to calculate the attenuation length. The measured attenuation length at 30 and 45 kHz is independent of the frequency within the uncertainties. Because Rayleigh scattering depends on grain

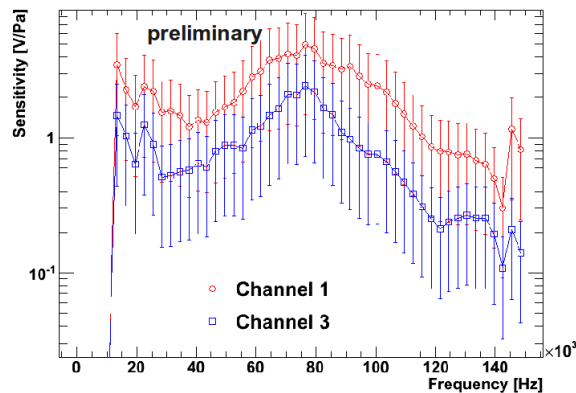


Figure 6: Absolute sensitivity in ice for two different SPATS sensor-channels

diameter and frequency, the measured attenuation length at the South Pole is not dominated by scattering.

3.5 SPATS sensor calibration

The SPATS sensor calibration was performed in the Aachen Acoustic Laboratory (AAL) as a complement to the in-situ test at South Pole with SPATS [14]. Sensor absolute sensitivity was measured in water and in ice using reciprocity calibration [15]. For this method, no absolute calibrated receiver is needed as reference. Fig. 6 shows the absolute sensitivity for two different SPATS sensor-channels in ice.

4 CONCLUSIONS

The South Pole Acoustic Test Setup has been operated successfully since January 2007 and has been able to measure or constrain all South Pole acoustic ice parameters. We presented the latest results from SPATS including:

- The sound speed depth profile was measured in deep ice and found to be consistent with a constant sound speed below 200 m depth. Further analysis is underway including inclined paths. This will allow us to probe the fabric of the ice because the sound speed can vary from site to site due to the difference in the crystal grain orientation.
- The absolute noise at the South Pole is very stable and Gaussian distributed. The measurements of the absolute noise level allow us to put a threshold for a future acoustic neutrinos detector at South Pole which depends on the noise level.
- SPATS identified sources for the transient noise, acoustic pulse-like events, in the IceCube detector volume and its vicinity.
- The attenuation length including the recent multi-frequency measurements is presented. The measurements do not show a strong depth dependency. The

attenuation length, which seems not to depend on scattering, has been found to be about 300 m. This is less than expected from theory. However, for 10^{18} eV neutrinos, the typical distance over which they can be detected is reduced only by a factor of about 2.

- A SPATS sensor has been absolutely calibrated by the reciprocity method in ice.

SPATS is continuing to take data. An upgrade of the DAQ software to read out all sensor channels simultaneously and to form a multiplicity trigger online, will increase the detector sensitivity. SPATS results show that the acoustic detection technique represents a promising tool to build a large hybrid (acoustic/radio) neutrino telescope in the South Pole ice. Individual hits from an acoustic array operated synchronously with a radio array could still be valuable. The coincidence between radio and acoustic hits could provide much-needed confirmation about the direction and energy reconstruction of the events.

5 ACKNOWLEDGMENT

We are grateful for the support of the U.S. National Science Foundation and the hospitality of the NSF Amundsen-Scott South Pole Station.

References

- [1] R. Engel et. al., Phys. Rev., 2001, **D(64)**:093010-1 - 093010-10.
- [2] D. Seckel, AIP Conf. Proc., 2001, **579**:196-203.
- [3] A. Achterberg et. al., Phys. Rev., 2007, **D(76)**:027101-1 - 027101-6.
- [4] G.A. Askaryan, Soviet Physics JETP-USSR, 1962, **14(2)**:441-443.
- [5] G.A. Askaryan et al., NIM, 1979, **164**:267-278.
- [6] P.B. Price, Astropart. Phys., 1996, **5**:43-52.
- [7] P. B. Price, J. Geophys. Res., 2006, **111(B02201)**:1-9.
- [8] D. Besson et. al., Int. J. Mod. Phys., 2006, **A(21S1)**:259-262.
- [9] Y. Abdou, et. al., submitted to NIM-A, arXiv:1105.4339v1.
- [10] J.-H. Fischer, 2006, Diploma thesis, Humboldt-Universität zu Berlin.
- [11] R. Abbasi, et. al., Astropart. Phys., 2010, **33**:277-286.
- [12] R. Abbasi, et. al., submitted to Astropart. Phys., arXiv:1103.1216v1.
- [13] R. Abbasi, et. al., Astropart. Phys., 2011, **34**:382-393.
- [14] T. Meures, L. Paul, and M. Ribordy, submitted to NIM-A, arXiv:1010.2313v2.
- [15] R. J. Urick.: 1983, Principles of underwater sound, 3rd ed., Peninsula Publishing.



The Radio Air Shower Test Array (RASTA) – enhancing the IceCube observatory

THE ICECUBE COLLABORATION¹, THE ARA COLLABORATION²

¹See special section in these proceedings

²See special section in these proceedings

Abstract: Radio detection offers the opportunity to measure cosmic ray induced air showers at greater than PeV energies via their electromagnetic emission in the MHz region. We intend to use this technique to extend the capability of the IceCube and IceTop detectors at the South Pole to measure cosmic ray observables. The radio emission is dominated by the electron contribution in the shower maximum, hence providing an integral measure of the shower development. It supplements the measurement of high energetic muons deep in the ice by IceCube and the sampling of the air shower on the surface by IceTop. Using these new, complementary observables, a radio extension can improve the measurement of the composition of cosmic rays. Further, the surface radio detector will increase the neutrino sensitivity of IceCube by providing a veto for air showers. It also may allow the study of photon induced air showers, which contain a smaller muon component than air showers induced by charged particles. We present simulation and experimental studies demonstrating the feasibility and providing a first impression of the physics potential of this approach.

Corresponding authors: Michael DuVernois² (duvernois@icecube.wisc.edu)

²Dept. of Physics, University of Wisconsin, Madison, WI 53706, USA

Keywords: Radio air shower detection; RASTA; IceCube; ARA; South Pole

1 Introduction

After first being discovered in the late 1960s [1], radio emission of air showers has again received increasing interest in the past years. This is mainly due to the achievements in information technology, which open the possibility to use phased arrays of radio antennas in combination with digital beam forming. Its main advantages are low cost and simple design of the radio antennas as compared to classical air shower detector elements (such as scintillators or photomultipliers) and the very large field of view provided by the phased array (usually close to 2π sr). A first proof of this technology has been provided by the LOPES experiment [2, 3], a prototype setup for LOFAR – a multi-site, multi-purpose radio telescope spanning half of Europe. Radio technology is today also being developed as an extension at many existing air shower experiments (KASCADE-Grande, Pierre Auger Observatory, Tunka, ...).

In this paper, we will first outline the physics motivation for an extension of the IceCube observatory with an extended $\mathcal{O}(10)$ km² radio array, then describe the current preparatory measurements, and finally outline a roadmap towards a prototype experiment at the South Pole: RASTA (Radio Air Shower Test Array), that will allow us to fully quantify the physics potential of a large scale radio extension for the IceCube observatory.

2 Physics Motivation

The all particle energy spectrum of cosmic rays follows a simple power law with two prominent changes in spectral index: a steepening at ~ 4 PeV, called the “knee” followed by a flattening at a few times 10^{18} eV, termed the “ankle”. The knee is believed to result from the cut-off in protons from galactic sources, while the region between knee and ankle would represent the dying out of heavier elements from galactic accelerators and the transition to an extragalactic component at the ankle. However, the chemical composition of cosmic rays in this energy range is not well constrained, yet. The composition is derived from the properties of cosmic ray induced extensive air showers. The two quantities sensitive to composition usually used are the depth of the shower maximum in the atmosphere X_{\max} (and the width of the X_{\max} -distribution) and the electron-to-muon ratio at ground level.

The IceTop 1 km² air shower detector [4], part of the IceCube observatory [5] located at the geographic South Pole, has an energy threshold of 300 TeV primary energy and can measure up to ~ 1 EeV where it becomes limited by statistics. We propose to enhance the IceCube observatory with a large area ($\mathcal{O}(10)$ km²) antenna field on the surface, centered at IceTop, to detect radio emission from air showers in the MHz frequency band. The envisioned radio detec-

tor is expected to have an energy threshold of $\mathcal{O}(10)$ PeV and its larger area will allow us to collect statistics up to higher primary energies, resulting in a significant overlap with the energy range accessible to the Pierre Auger Observatory. The range of cosmic ray primary energies covered by the enhanced IceCube observatory will in particular allow for measurements in the transition region between knee and ankle of the cosmic ray spectrum and will enable systematic studies and cross calibration between IceTop, the radio detector, and the Pierre Auger Observatory.

The IceCube observatory is a very well suited facility to study cosmic ray composition via the electron-to-muon ratio of air showers [6]. IceTop at the surface measures the charged particles at ground level while only high energy muons can penetrate through the Antarctic ice sheet and be measured in the deep in-ice detector. The radio signal gives an integral measurement of the electron component over the whole development of the air shower and the largest contributions are emitted in the shower maximum. The enhanced observatory would allow for three independent, coincident measurements of air showers—charged particles at ground level, high energy muons in-ice, and the radio signal emitted over the whole shower development—thus improving the knowledge about the primary particle. Studies on cosmic ray composition can be performed in two ways. First, for air showers where the muon bundle in the shower core penetrates the geometric volume of the IceCube in-ice detector, the amplitude of the radio signal on the surface can be used to estimate the electron number of the shower and thus its energy, while the muon number can be estimated from the in-ice signal. With this method a zenith range up to 60° can be covered with a radio array reaching out 3 km from the centre of IceTop. Second, the lateral distribution function of the radio signal is expected to be a composition sensitive variable [7, 8] which would allow for radio-only composition studies, largely increasing the aperture of the detector since no geometric overlap of the events geometry with IceCube is required. The first method described above would also allow us to explicitly search for UHE photons which manifest themselves as electromagnetic showers with no, or a very small, muon component in the deep in-ice detector.

Further, the increased area of the surface detector can be used as a veto against air shower muon bundles in the deep in-ice detector which are the main background channel in EHE neutrino searches in IceCube [9], increasing IceCube’s sensitivity to horizontal and down-going high energy neutrinos. An estimate shows that the sensitivity to cosmogenic neutrinos can be increased by a factor of more than three using a radio array extending 3 km around the centre of IceTop [10].

To proof the technical feasibility of such a large area radio detector and to quantify the physics potential more precisely the installation of the RASTA test setup is proposed (cf. Sec. 4). In parallel, to study the physics potential of the envisaged radio detector, a detector simulation chain based on CORSIKA [11] simulations, the air shower ra-

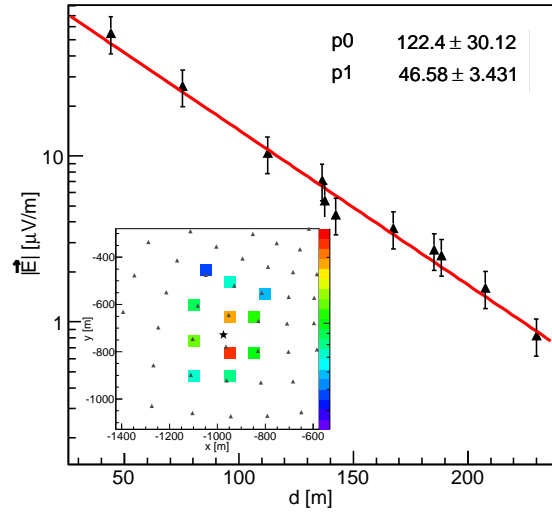


Figure 1: Radio signal strength as function of distance from the shower axis. The inset shows the distribution of recording antennas on the ground; the asterisk marks the position of the shower core. The origin of the coordinate system is located at the centre of IceTop.

dio emission code REAS3 [12], and the IceCube detector simulation software has been developed. This simulation chain allows for the uniform treatment of all three detector components and is currently used to study the energy threshold and composition sensitivity of different detector configurations. For simulations, a radial geometry reaching out to 4.5 km radius has been chosen for the antenna array, comprising a total of 1110 antennas. Since showers with their axis intersecting the geometric volume of the in-ice detector are most promising, the spacing between antennas increases from 80 m in the centre to 800 m at the outer circumference, taking into account the increasing zenith angle of these “golden events”. A typical simulated event, induced by a 10 PeV primary proton, is shown in Fig. 1 together with part of the simulated antenna array and the lateral distribution of the radio signal amplitude. The muon bundle from this air shower generated a signal in 571 optical modules of the deep IceCube detector.

3 Preparatory Measurements

One important ingredient for the simulation of a radio detector and the estimation of its sensitivity is the knowledge of the electromagnetic background conditions at South Pole station. This includes both, the continuous background noise and its variations on different time scales, and possible transient backgrounds. In the past several measurement campaigns have been performed [10, 13], which for technical reasons always took place close to South Pole station buildings and thus yielded only upper limits on the



Figure 2: ‘Fat Wire Dipole’ surface antenna deployed in the ARA test setup. The 3.7 m long antenna is made from copper pipes stabilized in a wooden frame.

noise conditions $\mathcal{O}(1)$ km away from all buildings, where a radio detector would be built.

In the austral summer 2010/2011 the ARA (Askaryan Radio Array) collaboration deployed a test setup [14] about 2.5 km away from South Pole station, outside the IceCube footprint. ARA is searching for Askaryan GHz radio emission in the ice from EHE neutrino interactions. Two DAQ channels of the test setup have been instrumented with 3.7 m dipole antennas on the surface (cf. Fig. 2) that are sensitive in the frequency range 25 – 160 MHz. The signal from the antennas is amplified with two low noise amplifiers (37 + 41 dB) and read out with 12-bit ADCs at a sampling rate of 1 GHz.

Minimum bias data recorded with the surface antennas of this setup allowed us to measure the power spectral density (PSD) of the electromagnetic background away from South Pole station in the frequency band from 25 – 160 MHz. Figure 3 shows the measured PSD (ARA channel 15 and 16) at the input of the ADC averaged over all data available from 18 January to 6 April 2011. For comparison a parameterization of the expected galactic noise (from [15]) and thermal noise folded with the ARA system response are shown. The antenna response has been simulated using NEC4 [16]. The data are well described by a superposition of galactic and thermal noise. The cut-off at ~ 30 MHz is suspected to be due to unaccounted features in the ARA system response.

The surface antennas have been deployed in air in a trench which will be snowed in during the year. This will allow us to study the difference in the antennas response on and under the snow surface in both data and antennas simulation and the long time performance of the antennas in the Antarctic environment.

Sensitivity of the setup to galactic noise can further be shown by analyzing the variation of the background noise during the sidereal day. At South Pole the galactic centre always has the same elevation but the antenna response is not uniform in azimuth. Figure 4 shows the RMS of the

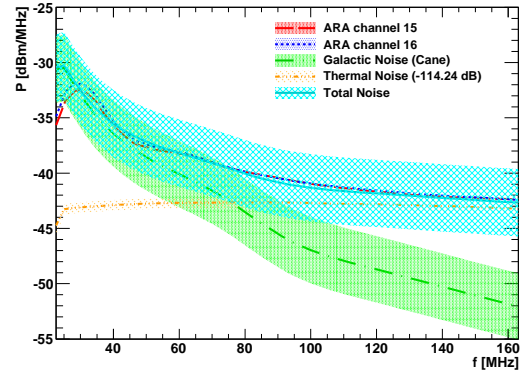


Figure 3: Time averaged background noise measured with the two ARA surface antennas. For comparison, the galactic [15] and thermal noise expectations, convoluted with the ARA amplification and system response, are shown.

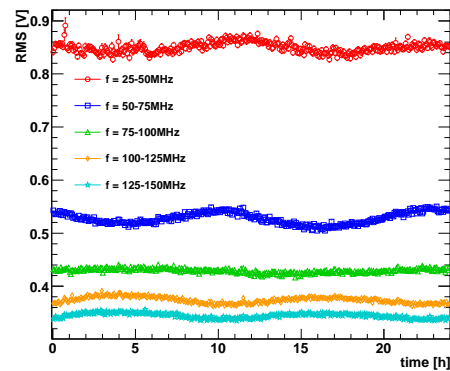


Figure 4: Modulation of the noise RMS in the surface antennas for different frequency bands during the sidereal day. See text for details.

background noise in ten minute bins modulo one sidereal day for different frequency bands. Following the symmetry of the antenna, two full oscillations are observed per day. The amplitude of the modulation decreases for higher frequencies as is expected from the galactic emission spectrum (cf. Fig. 3). At ~ 90 MHz the phase of the modulation is inverted. This effect is understood from simulations of the antenna response function.

During the austral winter 2011 a dedicated surface trigger in the ARA test setup will allow us to study transient backgrounds at South Pole far from the station buildings and the IceCube array.

4 Roadmap

Considering the restricted deployment cycle due to the remote location, a staged proposal spanning three years has been made. In the first year we will aim towards unambiguously establishing the detection of air showers above the

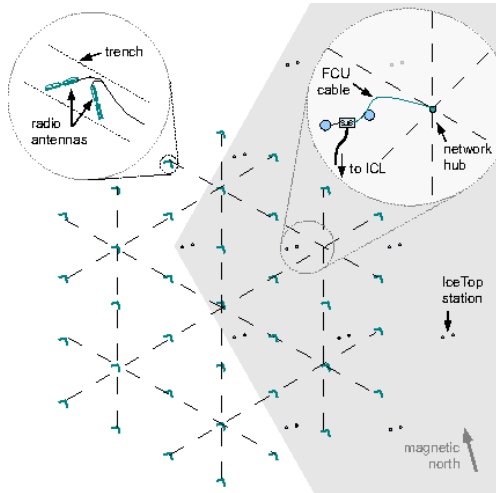


Figure 5: Possible configuration for RASTA having partial overlap with the IceCube footprint (gray shaded area). The configuration of the antenna pairs is shown in the upper left inset. The dashed lines indicate the data and power transmission network. The upper right inset illustrates the connection to the IceCube network using existing spare cables running to the IceTop stations.

background noise and provide a proof-of-viability for this detection technique in the Antarctic environment. Using a conservative estimate based on REAS2 [17] simulations, air showers with a primary energy of $E_{\text{prim}} > 10^{17}$ eV should be detectable at $> 5\sigma$ above the ambient noise level at a distance of 125 m [10]. Antennas will be deployed in orthogonally polarized pairs. Four such pairs forming an equilateral triangle with 95 m side length and one pair in its centre and requiring a three-fold coincidence will provide an effective area of $3 \cdot 10^4$ m². Using the charged cosmic ray flux as measured by the KASCADE experiment [18], each of these clusters will detect ~ 8 events per day. Even allowing for considerable inefficiencies (e.g. due to anthropogenic backgrounds), some 10^3 events will be accumulated per year.

In the second and third seasons all of the key technologies that are required for a several-km² array should be employed. This will also allow us to demonstrate the scalability of the approach. With a significantly larger number of antennas on an enlarged footprint, this second stage will collect a data sample large enough to allow detailed verification of the array performance and shower reconstruction. Figure 5 shows a possible setup for the third year stage of RASTA. Partial overlap with the IceCube footprint allows for coincident air shower measurements with IceTop and allows us to study both, influences of possible noise from IceTop and data measured at some distance to existing infrastructures.

5 Conclusions and Outlook

A large area surface radio detector is a promising enhancement for the IceCube observatory to study the composition of cosmic rays in the transition region from the knee to the ankle and improve IceCube's sensitivity to UHE neutrinos. A full detector simulation chain based on REAS3 has been developed and different detector configuration and their physics potential are presently studied. In-situ measurements of electromagnetic interference show promisingly low noise levels. A path towards RASTA, a full test setup to demonstrate the viability of a full detector, has been presented.

References

- [1] H. R. Allan, R. Clay, A. Jones et al., *Nature*, 1969, **222**, 635–637.
- [2] H. Falcke, P. Gorham, *Astropart. Phys.*, 2003, **19**, 477–494.
- [3] H. Falcke et al., *Nature*, 2005, **435**, 313–316.
- [4] IceCube collaboration, paper 0807, these proceedings.
- [5] H. Kolanoski, IceCube summary talk, these proceedings.
- [6] IceCube collaboration, paper 0923, these proceedings.
- [7] T. Huege, R. Ulrich, R. Engel, *Proceedings of the 30th ICRC*, 2007, arXiv:0707.3761 [astro-ph].
- [8] K. D. de Vries, A. M. van den Berg, O. Scholten et al., *Astropart. Phys.*, 2010, **34**, 267–273.
- [9] R. Abbasi et al. (IceCube collaboration), *Phys. Rev. D*, 2011, **83**, 092003.
- [10] J. Auffenberg: 2010, PhD Thesis, University of Wuppertal.
- [11] D. Heck, J. Knapp, J. N. Capdevielle et al.: Forschungszentrum Karlsruhe, FZKA 6019, 1998.
- [12] M. Ludwig, T. Huege, *Astropart. Phys.*, 2011, **34**, 438–446.
- [13] J. Auffenberg, D. Besson, T. Gaisser et al., *Proceedings of the 31st ICRC*, 2009, arXiv:1007.3925 [astro-ph.IM].
- [14] P. Allison et al. (ARA collaboration), arXiv:1105.2854 [astro-ph.IM].
- [15] H. V. Cane, *Mon. Not. R. Astr. Soc.*, 1979, **189**, 465–478.
- [16] G. J. Burke, Lawrence Livermore National Laboratory, 1992.
- [17] T. Huege, R. Ulrich, R. Engel, *Astropart. Phys.*, 2007, **27**, 392–405.
- [18] H. Ulrich et al., *Nucl. Phys. B. Proc. Suppl.*, 2003, **122**, 218–221.



IceCube's In Ice Radio-Frequency extension

THE ICECUBE COLLABORATION¹, E. CHENG², L. RUCKMAN³, G.S. VARNER³

¹See special section in these proceedings

²Dept. of Physics, Univ. of Wisconsin, Madison, WI 53703, USA

³ Dept. of Physics and Astronomy, Univ. of Hawaii, Manoa, HI 96822, USA

Abstract: In preparation for designing a large scale array sensitive to high energy neutrinos (EeV), several Radio Frequency (RF) detectors and calibration equipment were installed with the IceCube neutrino detector at the geographic South Pole between the years 2006–2010. The wide and deep holes drilled for IceCube provided a unique opportunity for deep-ice RF detection studies at depths never surveyed before. The deployed detectors are installed between 5 to 1400 meters deep in the ice, and are sensitive to frequencies in the range of 200 MHz–1 GHz. We will present results of ice properties studies (attenuation length and index of refraction) and environmental noise study.

Corresponding authors: Hagar Landsman(hagar@icecube.wisc.edu), Mike Richman(mike.d.richman@gmail.com), Kara Hoffman(kara@umd.edu)

Keywords: Neutrino, Askaryan, GZK, South Pole, ice properties, attenuation

1 Introduction

The concept of high energy neutrino radio frequency detector buried in ice at shallow depths or deployed as a surface array was suggested nearly 30 years ago [1]. The RICE [2] array and the ANITA experiment [3] are already taking advantage of the Askaryan effect and the massive volume of ice in Antarctica for neutrino detection by looking for the coherent radio Cherenkov emission from charge asymmetry in high-energy neutrinos cascades. Future experiments include ARIANNA [4], a surface array on the Ross Ice Shelf, and ARA [5], an in-ice array at shallow depths near the South Pole. Our unique access to IceCube's deep and wide holes have provided us with an opportunity for deploying radio frequency (RF) detectors in the deep Polar ice. These detectors use the communication and time calibration systems developed for IceCube and rely on the experience within the IceCube Collaboration for developing hardware and software and for building and deploying highly-sensitive equipment in the extreme South Pole environment as well as on radio technology expertise from the RICE and ANITA Collaborations. IceCube's deep holes and well-established data handling system provide a unique opportunity for deep-ice RF detection studies.

2 Hardware description

2.1 Full digitization detectors

IceCube's radio extension modules, consisting of several radio frequency (RF) detectors as well as calibration equipment, were installed on IceCube strings during the austral summers between 2006 and 2010 at depths of 5 to 1400 m. Each radio module was installed directly above IceCube's digital optical modules (DOMs). The RF components were mechanically attached to the ~ 3 km-long IceCube main cable (a 5-cm-diameter cable bundle for communication and power) which simply served as a mechanical support; some of the modules, however, were tapped into one of the auxiliary twisted-pairs within the main cable designed for specialized device operations. The main cable, being a massive conducting object, can shadow the RF antennas.

During the first two seasons five detectors capable of full waveform (WF) digitization were deployed. These so called "clusters" consist of four receiving channels equally spaced over ~ 40 m along the IceCube cable, a transmitting channel and a central electronics module. Each receiver channel consists of a broadband dipole antenna (with the gain centered at ~ 400 MHz in air and ~ 250 MHz in ice), and a set of front-end electronics (housed in a metal tube), including filters (450 MHz notch filter for rejecting constant interference from the South Pole commu-

tion channel, and 200 MHz high-pass filter) and amplifiers (~ 50 dB low-noise amplifier). An additional ~ 20 dB amplification is done at a later stage within the electronic module for a total amplification of ~ 70 dB. A schematic of the 2006–2007 cluster is shown in Figure 1. Three clusters were deployed at depth of ~ 300 m, and two at ~ 1400 m. A detailed description of the electronics installed inside the DRM can be found elsewhere [6, 7].

2.2 Transient detectors

The idea of using an array of simple transient sensors to image the unique spatiotemporal signature of neutrino interactions in Antarctic ice was proposed by Gusev and Zheleznykh nearly thirty years ago [1]. In this type of detector system, the pattern of coincident hits among a large number of sensors provides event confirmation, indication of direction and energy, and information for rejecting sporadic noise on the basis of time-of-arrival and amplitude. Six units of transient-prototype-detector were deployed in the 2009–2010 season. Each unit consists of a discone wide-band omni-directional antenna feeding into a Transient Detector Assembly (TDA), an exploratory device, whose block diagram is shown in Figure 1. Each unit is read out using a control motherboard (MB) developed for the IceCube DOM [8]. The IceCube cable and calibration system also facilitates timing calibration and data handling. The units were deployed in pairs above three IceCube strings, with one unit at $z = -5$ m and the other at $z = -35$ m. The Local Coincidence (LC) capabilities of the IceCube MB are also exploited; when LC is enabled, each TDA pair reads out data only if both units in the pair are triggered in some adjustable time window. The rise-time of the output pulse from these units is on the order of 10–20 ns and is largely independent of amplitude.

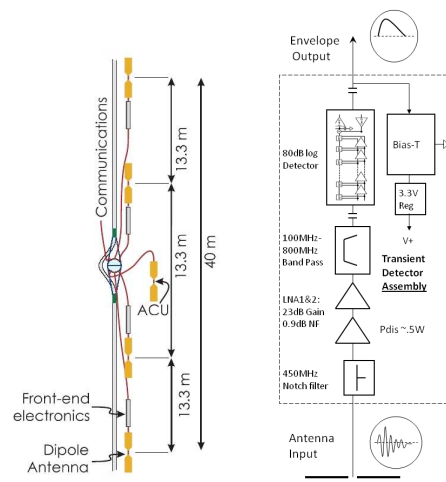


Figure 1: The radio cluster, consisting of the DRM (Digital Radio Module), 4 receiving antennas and 1 transmitting antenna (left); Block diagram of the Transient Detector Assembly (right).

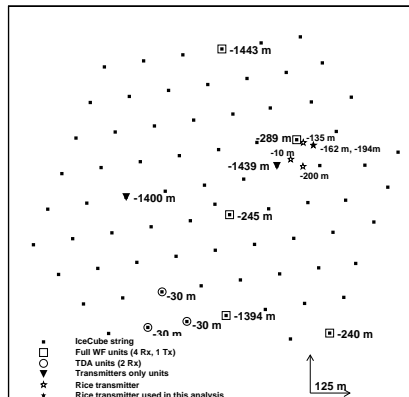


Figure 2: Map of the IceCube radio detector deployments, plotted on top of the full IceCube array. Also shown are the deployment depth of each unit relative to the surface, and the location of the RICE transmitters.

Figure 2 summarizes the in-ice locations and depths of the deployed units.

3 Ice Properties

The properties of ice at radio frequencies determine the feasibility and design of future GZK neutrino detectors. Specifically, the attenuation length affects the spacing between channels and the effective detector volume, whereas uncertainties in the index of refraction determine the reconstruction capabilities and simulation quality.

3.1 Attenuation Length

The attenuation length λ is the distance over which the signal amplitude diminishes by a factor of e due to absorption and/or scattering. In general, λ varies with the density and temperature of a medium and with the frequency of the radiation. In South Pole ice, the density and temperature vary with the depth z , and so the attenuation length is also a function of depth.

The previous in-ice RF attenuation data from the South Pole were obtained by sending signals down into the ice using a surface transmitter and recording the signals reflected from the bedrock below. This measurement provided an average RF attenuation over the round-trip, weighted by the temperature profile along the path [9].

The IceCube Radio Extension provides us with the first opportunity to make a point-to-point attenuation measurement independent of the unknown bedrock reflection coefficient. Of 20 available receiver channels, we use the 6 which have similar amplifiers and electronics. Our sources are RICE antennas which transmit signals from a pulser operated in an on-site lab. The pulse power can be varied by inserting attenuators in the line. The transmitting antennas are similar to the receiving antennas and are located at var-

ious depths down to 220 m, and up to ~ 1400 m away from the receivers (see Figure 2).

The simplest possible relative attenuation measurement would involve broadcasting a signal and measuring the relative power received by antennas at different distances from the transmitter. However, IceCube Radio Extension digitizers have insufficient dynamic range for this approach. Thus, we instead vary the transmitter power, measuring the values which yield the same power at different receivers. The differences between these values are $\Delta\mathcal{L}_{\text{total}}$, the total receiver–receiver difference in losses.

We assume that (in a logarithmic scale) $\Delta\mathcal{L}_{\text{total}} = \Delta\mathcal{L}_{\text{dipole}}(\theta) + \Delta\mathcal{L}_{\text{free space}}(\vec{r}, n(z)) + \Delta\mathcal{L}_{\text{attenuation}}(\vec{r}, \lambda)$. We use a standard dipole pattern for transmitters and receivers: $I(\theta) = (3/8\pi)I_0 \sin^2(\theta)$. The free space losses, which for uniform index of refraction would give the inverse square law, are calculated using ray tracing simulation. After obtaining $\Delta\mathcal{L}_{\text{total}}$ from measurement and $\Delta\mathcal{L}_{\text{dipole}}$ and $\Delta\mathcal{L}_{\text{free space}}$ from simulation, we can calculate the path-averaged attenuation length $\langle\lambda\rangle$: $\Delta\mathcal{L}_{\text{attenuation}} = 10 \log_{10} e^{-2\Delta r/\langle\lambda\rangle}$. Figure 3 shows the measurement of pulses from a RICE transmitter. Deep receiver channels show a linear response. Shallow receiver channels have a flatter response for higher power due to saturation; however, for sufficient transmitter attenuation, they also have a linear response.

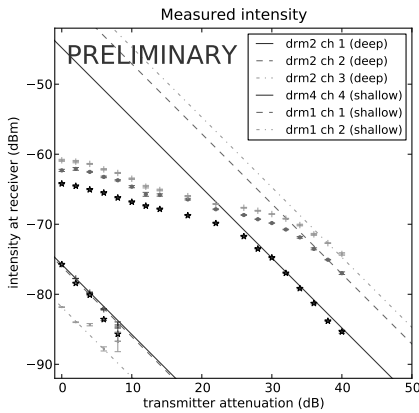


Figure 3: Measured intensity vs. transmitter attenuation.

A linear fit with a slope of -1 is done for the linear region on each curve. The difference between the x -intercepts for any pair of fits is equal to $\Delta\mathcal{L}_{\text{total}}$ for that antenna pair. To date, sufficient data has been taken only with one of RICE transmitters. Preliminary values obtained from this data for $\langle\lambda\rangle$ range from 400 to 700 meters. These numbers are somewhat lower than past results [9]; however, preliminary systematic error estimates suggest that these results will not be inconsistent with each other.

This measurement is ongoing. Our simulation of the effects of reflection and shadowing by an IceCube cable in the vicinity of a broadband dipole antenna is not yet complete.

Other remaining work includes estimating other systematics such as receiver gain uncertainties; taking data with additional transmitters; and combining results for $\langle\lambda\rangle$ with existing density and temperature measurements to obtain a model for $\lambda(z)$.

3.2 Index of refraction

Uncertainties in index of refraction lead to uncertainties of the order of a few ns in the time difference measured between two receivers a few meters apart (geometry-dependent); therefore, a precise knowledge of index of refraction is necessary for a sub-ns-resolution detector. The latest index of refraction measurement at the South Pole reported in [10] combines results using the RICE array down to 150 m and ice cores down to 240 m. The model used is of the form $n(z) = n_{\text{deep}} + (n_{\text{shallow}} - n_{\text{deep}})e^{n_c z}$, where $n_c \approx -0.0132 \text{ m}^{-1}$, $n_{\text{deep}} \approx 1.78$, and $n_{\text{shallow}} \approx 1.35$. The changing index of refraction causes rays to curve in the ice layers, especially in the soft ice layers on top of the glacier (firn), and decreases the angular acceptance of shallow-deployed detectors by causing total reflection of rays propagating between the layers. When looking at possible paths connecting a transmitter and a receiver both in ice there will be either zero or two solutions (direct ray and reflected ray) to the ray-tracing problem. The reflection takes place at the ice-air boundary on the surface, as illustrated in Fig. 4A.

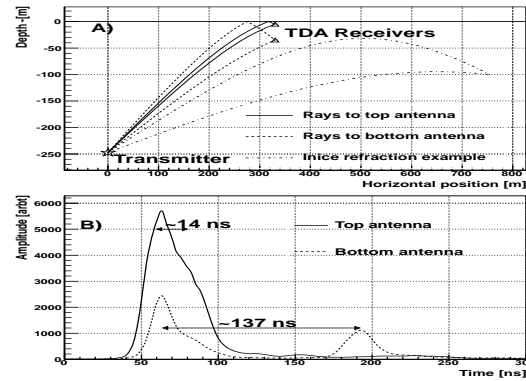


Figure 4: A. Ray Tracing showing the direct- and reflected-rays solutions. The depths and separation between the transmitter and the receivers in this figure correspond to the transmitter-receivers used in the analysis. B. Average WF collected on the top (solid) and bottom (dashed) antennas of the transient detectors. The time delay between the direct and the refracted ray detected by the bottom antenna is consistent with simulations (137 ns).

The extremely shallow location of the TDA units makes them sensitive to small variations in the index of refraction model, especially to n_{shallow} and n_c . Five out of six TDA units were able to trigger on a calibration pulse transmitted by a calibration antenna from depth of -245 m. The sixth unit that did not see the pulser (Top antenna at hole 8) was

in the shaded area where no solution exists. Limits on the ice model parameters can be set by measuring the trigger time differences between different units as well as the time differences between the direct and reflected ray. This is illustrated in Fig 4B where an average WF from a pulsar run for the top and bottom detectors is shown. The expected time delay between the direct and reflected ray for the top antenna was calculated to be about 14 ns, and the direct and reflected peaks are not resolvable. For the bottom antenna the simulated time delay was about 137 ns, in good agreement with the measurement. Figure 5 shows preliminary constraints on n_{shallow} and n_c based on combined time differences measured between detectors.

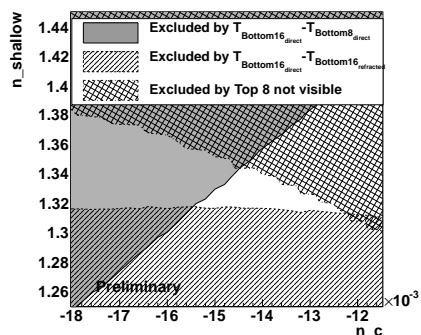


Figure 5: Excluded parameters space for index of refraction based on time delays between hits. This area includes systematic uncertainties from the following uncertainties: timing resolution, slewing, geometry and n_{deep} .

4 Environmental Noise

We have previously shown that timing of elevated noise rates coincided with the periods of winds stronger than ~ 20 knots (see Figure 6). Since the South Pole is electrically insulated, electrostatic charge accumulates easily, leading to a discharge causing EMI. There are two possible mechanisms as to how electrostatic charge builds up in strong winds: “precipitation charging” [11] where blowing snow causes structures to charge up; and “snowstorm electrification” [12], where charge separation occurs near the snow surface. A preliminary reconstruction study has pointed to an area around large structures in the Dark Sector as the origin of this interference. Preliminary studies with radio detectors away from the station have shown no such interference, supporting the assumption that the noise is originating from structures and not spontaneous charging of the ice. However, additional data are required since this analysis was performed early in the austral winter, using limited statistics [5].

We were also sensitive to weather balloon launches, happening twice a day. Since this noise source is well defined in time and frequency, it will not be a problem for future detectors.

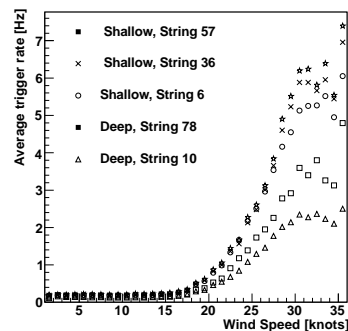


Figure 6: Average trigger rate vs. wind speed for the five clusters described in Section 2.1. The meteorological data were taken from the “Clean Air” automatic weather station, operated by The Antarctic Meteorological Research Center (AMRC) and the Antarctic Automatic Weather Station (AWS) Program [13].

5 Summary

IceCube’s mature drilling and data acquisition technology have facilitated the deployment of the first fully digital radio test equipment in South Pole ice as well as deployment to greater depths in South Pole ice than was previously possible. Using the IceCube radio frequency extension, we have obtained tighter constraints on the index of refraction model parameters, and an attenuation length measurement is also underway. We have also been able to characterize and understand the RF noise environment at the Pole. This information will provide a valuable guide for the design of a future GZK neutrino detector.

References

- [1] G. A. Gusev, I. M. Zheleznykh, JETP Lett. 38 (1983) 611–614.
- [2] I. Kravchenko, et al., Phys. Rev. D73 (2006) 082002.
- [3] P. W. Gorham, et al., Phys. Rev. D82 (2010) 022004.
- [4] L. Gerhardt, et al., arXiv:1005.5193.
- [5] P. Allison, et al., arXiv:1105.2854.
- [6] H. Landsman, et al., Nucl. Instrum. Meth. A604 (2009) S70–S75.
- [7] H. Landsman, et al., Nucl. Instrum. Meth. In Press, accepted manuscript, (2010) doi:10.1016/j.nima.2010.11.144.
- [8] R. Abbasi, et al., Nucl. Instrum. Meth. A601 (2009) 294.
- [9] S. Barwick, et al., J. Glaciology 51 (173) (2005) 231.
- [10] I. Kravchenko, et al., J. Glaciology 50 (171) (2004) 522.
- [11] S. B. Dunham, J. Atmospheric Sciences 23 (1966) 412.
- [12] M. Gordon, P. Taylor, Boundary-Layer Meteorology 130 (2009) 97–115.
- [13] ftp://amrc.ssec.wisc.edu/pub/southpole/surface_observations.



First Step Towards A New Proton Decay Experiment In Ice

THE ICECUBE COLLABORATION¹, CLAUDIO KOPPER²

¹See special section in these proceedings

²NIKHEF, 1098 XG Amsterdam, Netherlands

Abstract: Grand Unified Theories (GUTs) predict a finite lifetime for the proton. The most recent limit, reported by Super-Kamiokande for a $172.8 \text{ kTon} \times \text{year}$ exposure, on the proton decay partial lifetime ($p \rightarrow \pi^0 + e^+$) corresponds to 1.01×10^{34} years. In the supersymmetric extensions of SU(5), the lifetime of the proton is expected to be lower than 10^{36} years. To reach 10^{36} years sensitivity to proton decay requires a detector with a volume on the megaton scale sensitive to sub-GeV energy. Where and how such a detector might ever be realized remains an open challenge. Installation of massive detectors underground is presently a technological challenge with costly excavation, engineering and installation. We consider here the ice cap at the South Pole which might provide an alternative scenario for a megaton ring imaging Cherenkov experiment in the search for proton decay. The ice, studied by the IceCube Collaboration, is measured to be extremely pure and transparent. Further, IceCube has demonstrated the ability to instrument a detector volume at the gigaton scale on-schedule and on-budget. The 86 strings of IceCube photosensors provide sensitivity to particle interactions with energies between tens of GeV up to extremely high energies. Given the success of the IceCube project in instrumenting the world's largest Cherenkov neutrino detector, and the DeepCore sub-array to extend the reach to low-GeV physics, it seems reasonable to consider the question if the same principle of IceCube, using the Cherenkov medium as the detector support infrastructure, could provide a cost effective and simplified path to instrument megaton scale detectors with sufficient photocathode area to permit a viable proton decay experiment sensitive to 10^{36} year lifetime and beyond. In this paper we present the very first steps of a developing design study for a proton decay detector to be potentially deployed in the center of IceCube-DeepCore, based on Geant4 and the IceCube software with realistic optical properties of the glacial ice.

Corresponding authors: Darren Grant³ (drg@ualberta.ca), Per Olof Hulth⁴ (hulth@physto.se), Claudio Kopper⁵ (claudio.kopper@nikhef.nl), Sirin Odrowski⁶ (sirin.odrowski@mpi-hd.mpg.de), Elisa Resconi⁷ (elisa.resconi@tum.de), Martin Wolf⁶ (martin.wolf@mpi-hd.mpg.de)

³University of Alberta, Alberta, Canada

⁴Stockholm University, 10691 Stockholm, Sweden

⁵NIKHEF, 1098 XG Amsterdam, Netherlands

⁶Max-Planck-Institut für Kernphysik, 69117 Heidelberg, Germany

⁷TU Munich Excellence Cluster Universe, 85748 Garching, Germany & Friedrich-Alexander Universität Erlangen-Nürnberg, 91058 Erlangen, Germany

Keywords: proton decay; South Pole; IceCube; simulation; GEANT4; GENIE; GPGPU photon tracking

1 The Search for Proton Decay

In Grand Unified Theories (GUTs), introduced by Georgi and S.L. Glashow in 1974 [1], baryon number violating processes, like proton decay, are allowed. A favored predicted proton decay channel, by the minimal SU(5) gauge symmetry, is the decay into a neutral pion and a positron, where the neutral pion subsequently decays into two gammas. If the proton decays inside a volume of ultra-pure and transparent water (or ice), the decay products may be detected by observing the induced Cherenkov light cones, see Figure 1. Such a detection strategy is used by the Super-Kamiokande water Cherenkov experiment. The most recent limit on the proton lifetime decaying into the

“golden” channel, $p \rightarrow \pi^0 + e^+$, by the Super-Kamiokande Collaboration corresponds to 1.01×10^{34} years [2]. This result, based on 12 years of data taken between 1996 and 2008, already constrains part of the supersymmetry parameter space allowed by SU(5) supersymmetric extension. In this paper we report first steps towards a new idea for a proton decay experiment at the few megaton scale. The detector material we investigate here is the deep Antarctic glacial ice at the South Pole to be potentially instrumented with novel optical modules deployed inside the existing IceCube-DeepCore fiducial volume. The deployment strategy we consider is the one used by IceCube, namely strings of photo-sensors in holes drilled with hot water.

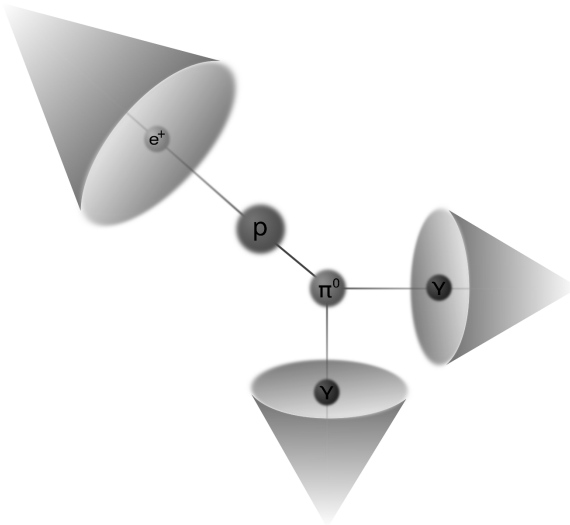


Figure 1: Artist's view of a proton decaying into a π^0 ($\gamma\gamma$) and a e^+ . Shown in the figure are the Cherenkov cones that result from interactions involving the final states of the decay products.

2 The IceCube Neutrino Observatory

IceCube is the world's largest neutrino detector. It is situated close to the geographic South Pole at the Amundsen-Scott South Pole Station. With an instrumented volume of roughly one gigaton, it is the most sensitive neutrino detector in a wide energy range, from tens of GeV up to the EeV scale. The detector operates on the principle of measuring the Cherenkov radiation emitted by charged particles, which have been produced in neutrino interactions. The measurements are taken with optical sensors (Digital Optical Modules, DOMs) deployed at depths between 1450 m and 2450 m, positioned along cables, called strings. IceCube consists of 86 such strings in a configuration of 78 laid out in a hexagonal grid with an inter-string spacing of 125 m and 8 DeepCore strings located at the center of the grid with an inter-string spacing of 40 m to 72 m. Each string of the standard IceCube configuration is equipped with 60 DOMs with a uniform DOM spacing of 17 m, covering a volume of $\approx 1 \text{ km}^3$. The DeepCore strings are equipped with 60 DOMs with high quantum efficiency PMTs and with a denser spacing of 10 m in the upper part (1,750 m - 1,850 m) and 7 m below 2,100 m. With the dense instrumentation in the deepest, clearest ice and use of the high quantum efficiency PMTs, DeepCore aims to achieve trigger threshold for muon neutrinos of $\approx 10 \text{ GeV}$ [3].

2.1 The South Pole Ice as Detector Material

The optical properties of the deep ice at the South Pole are excellent with a measured scattering length in the range 40-70 m and a maximum absorption length of about 200 m

measured at 400 nm (see [4] and Figure 8 in [5]). The clearest ice is found at depths below $\approx 2,100 \text{ m}$ [5]. We note that the wavelength dependence for scattering and absorption length are incorporated in the simulation reported here just as they are in the IceCube general simulation chain. The site is characterized by exceptional operational conditions, including high radiopurity and low stable temperature. In this environment the IceCube optical modules operate with very low noise, providing an average dark noise rate of 400 Hz [6] and a somewhat higher rate in the DeepCore higher quantum efficiency modules.

The installation of additional future detector components could follow the well established deployment methods used for IceCube strings, exploiting the ice cap as both Cherenkov medium and support infrastructure for the detector elements. IceCube has already successfully demonstrated the ability to instrument a gigaton-scale volume water Cherenkov detector within prescribed schedule and budget constraints. If the concept of Cherenkov ring reconstruction in the ice proves feasible, the underground physics community would have an attractive alternative to the daunting technological challenge of preparing few MT-scale deep caverns for next generation experiments.

The proposed location for a new detector, at the center of the IceCube-DeepCore ice bound arrays, would benefit from an active veto against muons induced by cosmic rays. DeepCore has already demonstrated the usability of IceCube as an efficient muon veto: as reported in more detail in [8], a muon background rejection of about $8 \cdot 10^{-3}$ [7] for the overall IceCube trigger ($\sim 2700 \text{ Hz}$) is achieved with an on-line filter algorithm. Novel muon reconstruction methods, currently under investigation, are expected to provide an overall muon rejection efficiency of the order 10^{-6} [9]. Further, the inclusion of the DeepCore array in such a veto scheme is expected to enhance the efficiency for future low-energy detector installed in the ice. Although cosmic muons, and the spallation products they produce, are likely not the crucial background for the $p \rightarrow \pi^0 + e^+$ channel (as shown by Super-Kamiokande we expect the main background to be atmospheric neutrino interactions [10]) the veto does provide valuable information to identify activity in the detector with an expected minimal impact on detector deadtime.

3 Proton Decay Simulation

A first challenge, discussed here, concerns establishing a robust Monte Carlo simulation which can provide the necessary information to initiate a full design feasibility study. Dedicated software for the simulation of proton decay events has been developed that combines Geant4 [11], [12] with a custom GPU-enabled simulation algorithm for photon propagation based on the IceCube software called IceTray [13]. Geant4 is used to simulate the particle cascade starting from the decay products of the proton, e.g. π^0 and e^+ . Integrating already existing or new Geant4 simulation code into IceTray, and to additionally add parallel process-

ing support to Geant4, required development of a suite of tools. This suite includes a photon propagation algorithm that takes into account the optical properties of the deep glacial ice at the South Pole. Scattering and absorption are modeled using horizontal ice layers with properties derived from measurements taken by IceCube [4]. Photon propagation is one of the most computationally intensive tasks during event simulation and thus its optimization is highly desirable. Since all photons are independent and may be treated in exactly the same way, the algorithm lends itself for implementation on dedicated parallel multiprocessors, e.g. Graphics Processing Units (GPUs). One such implementation, using OpenCL [14], was developed specifically for this task. Cherenkov photon-emitting particle steps from Geant4 are collected and provided in bunches to the GPU where, in turn, photons are generated according to the Cherenkov spectrum. The photons are propagated through the detector medium until either absorbed or incident on an optical module. In the latter case, all photon properties are stored for post-processing. After propagation, information on the incident photons is transferred to the host PC and used to generate hits. Decoupling hit generation from photon propagation permits different optical module design choices to be easily evaluated. We note that, while not the focus of this particular paper, the simulations for the critical atmospheric neutrino background events will use the GENIE software package [15] which is currently being incorporated into the IceCube simulation chain.

A first study is now underway with an idealized strawman detector, see Figure 2. The goal of such a geometry is to make it straightforward to optimize the detector geometry for proton decay. The idealized detector consists of a cylindrical arrangement of 235 strings where each string on a ring has a distance of ≈ 5 m to its neighboring strings of the same ring and the neighboring rings have a distance of 15 m to each other. We note that the 5 m distance of closest approach for the strings assumes no further improvement in the IceCube method of drilling. In the strawman design each string has 400 optical modules, spaced evenly over 400 m. The simulation has the ability to consider a variety of optical sensor technologies; from the standard IceCube digital optical modules, of which more than 5000 are currently successfully operating deep in the ice, to new multi-PMT modules [16] that have the potential to significantly increase the photocathode coverage.

4 Beyond IceCube

The goal to achieve a sub-GeV energy threshold inside the Antarctic ice requires a very densely instrumented detector compared to IceCube-DeepCore. First steps towards a better understanding of the feasibility of such sub-GeV detector is now underway. Interest in such a detector includes many members of IceCube and groups from the broader community. An informal collaboration named PINGU, for ‘‘Phased IceCube Next Generation Upgrade,’’ has been formed in order to provide a framework for the

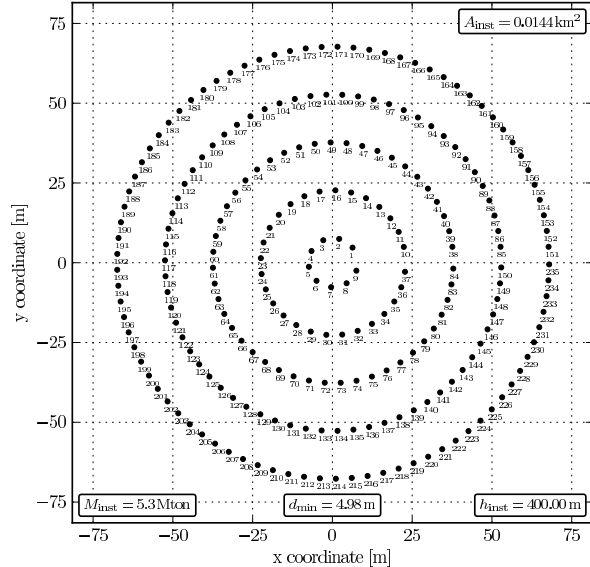


Figure 2: The geometry of the idealized proton decay detector used for this simulation study here reported.

design and R&D studies connected to future opportunities for astroparticle physics at the South Pole. A first informal PINGU workshop took place in Amsterdam in March 2011 (<http://www.nikhef.nl/pub/conferences/icecube/pingu/>).

The simulation tools we have introduced in this paper provide an effective starting point for determining the feasibility of an ice bound proton decay detector. As part of the ongoing study, different geometries of strings and photon sensors are considered. Particular attention at the current stage is paid to the effective photon coverage of the designs, which includes the photocathode coverage and quantum efficiency for the sensors as well as a comprehensive study of the background induced by atmospheric neutrinos. An ambitious goal has been set to test the feasibility for designing a 5 MT ice ring-imaging Cherenkov detector (1.6×10^{36} protons). The strategy aims to be competitive in terms of budget, in particular considering infrastructure costs, instrumented volume and time-line with respect to other existing design studies like for example [18, 19, 20]. The Super-Kamiokande detector collects approximately 7 p.e. per MeV deposited for a wavelength range of 350 nm to 500 nm [17] in order to reconstruct neutrinos of solar origin to energies below 5 MeV. The detector contemplated here would need to achieve a photon collection efficiency sufficient to image rings at the higher energies relevant for proton decay. In doing so, and assuming the dominant atmospheric neutrino background levels are the same, one arrives at a potential scenario for $\sqrt{N_{bkgd}}$ improvement in sensitivity for the increased fiducial volume.

196 **References**

- 197 [1] H. Georgi, S.L. Glashow, Phys. Rev. Lett., 1974, vol.
198 32(8): 438-441
- 199 [2] The Super-Kamiokande Collaboration, 2010,
200 [http://www-sk.icrr.u-tokyo.ac.jp/whatsnew/new-](http://www-sk.icrr.u-tokyo.ac.jp/whatsnew/new-20091125-e.html)
201 20091125-e.html
- 202 [3] The IceCube Collaboration, arXiv:0907.2263
- 203 [4] M. Ackermann *et al.*, J. Geophys. Res., 2006, vol. 111:
204 D13203
- 205 [5] The IceCube Collaboration, paper 0333, these pro-
206 ceedings
- 207 [6] The IceCube Collaboration, NIM A 618 (2010) 139-
208 152
- 209 [7] D.J. Koskinen (for the IceCube collaboration), Nucl.
210 Phys. B Proc. Suppl., in press
- 211 [8] The IceCube Collaboration, paper 0329, these pro-
212 ceedings
- 213 [9] O. Schulz, S. Euler, and D. Grant [The IceCube
214 Collaboration], Proceedings of the 31st ICRC, LODZ,
215 POLAND, 2009
- 216 [10] A. Rubbia, arXiv:0407297v1, figure 3
- 217 [11] S. Agostinelli *et al.*, Nuc. Instr. Meth A 506 (2003)
218 250-303
- 219 [12] IEEE Transactions on Nuclear Science 53 No. 1
220 (2006) 270-278
- 221 [13] T. DeYoung, CHEP2004 Int. Conference, 2004, pro-
222 ceedings: 463-466
- 223 [14] Khronos OpenCL Working Group: 2008, The
224 OpenCL Specification, ed. A. Munshi, Khronos
- 225 [15] C. Andreopoulos *et al.*, Nucl. Instrum. Meth., 2010,
226 vol. A614: 87-104
- 227 [16] P. Kooijman, Nucl. Instrum. Meth., 2006, vol. A567:
228 508-510
- 229 [17] A. Rubbia, arXiv:0407297v1, page 5
- 230 [18] Y. Suzuki, Second International Workshop on
231 Neutrino Oscillations and their Origin, arXiv:hep-
232 ex/0110005
- 233 [19] K. Nakamura, Int. J. Mod. Phys. A 18, 4053 vol. 18
234 no. 22 (2003)
- 235 [20] S. Raby *et al.*, arXiv:0810.4551